Dynamic Light Scattering from Semidilute Solutions of a Styrene−Acrylonitrile Random Copolymer

Haifeng Zheng and Iwao Teraoka*

Herman F. Mark Polymer Research Institute, Polytechnic University, Six MetroTech Center, Brooklyn, New York 11201

Received September 22, 2000; Revised Manuscript Received June 8, 2001

ABSTRACT: Dynamics of a random copolymer, poly(styrene-*co*-acrylonitrile), in dilute and semidilute solutions was studied by using dynamic light scattering. The solvent used was a mixture of dioxane and acetonitrile (ACN). The mixing ratio and the temperature were changed to provide the copolymer with various solvent conditions that range from a good to a Θ solvent. At low ACN contents, the autocorrelation function of the light scattering intensity had a single relaxation mode. Its diffusion changed from the mutual diffusion to the cooperative diffusion of entangled chains in the good solvent as the concentration c increased. At high ACN contents (near Θ), the diffusion coefficient decreased to $^1/_3$ of the dilute solution value and the scattering intensity increased almost linearly with c, before the diffusion coefficient turned to increase as $\sim c$ and the scattering intensity to decrease as $\sim c^{-1}$, indicating the cooperative diffusion of entangled Θ chains. In this high concentration range, the autocorrelation function exhibited a slow diffusion mode as well. A high friction coefficient and an extended near-linear range in the scattering intensity, especially at low temperatures, suggest dynamic clustering of chains upon increasing the concentration.

Introduction

Dynamic light scattering (DLS) is a powerful tool to investigate various fluctuations in concentrated solutions of polymer.[1] Recent studies focused on nonsimple systems such as solutions of a diblock copolymer in a nonselective solvent in the disordered state[2−5] and ternary solutions of two homopolymers in a common solvent.[6−13] It is common to these systems that the DLS autocorrelation function exhibits fast and slow diffusion modes. The fast mode becomes faster and the slow mode becomes slower as the polymer concentration increases. The fast mode is due to local monomer density fluctuations and is essentially the same as the cooperative diffusion universally observed in semidilute solutions of a homopolymer. The slow mode, called a heterogeneity mode, is ascribed to self-diffusion modulated by a thermodynamic function that goes to zero as the solution approaches a critical point of micro- or macrophase separation.[2,5−7] In the semidilute solution of a diblock copolymer, an additional, scattering angle-independent mode was observed and ascribed to an internal relaxation of the chain conformation.

Recently, Koňák et al.[14−16] studied semidilute solutions of poly(styrene-*co*-methyl methacrylate) by using DLS. In benzene isorefractive with poly(methyl methacrylate) (PMMA), slow diffusion was observed in addition to the fast cooperative diffusion.[14] The relative height of the slow mode in the DLS autocorrelation function increased as the average composition of the copolymer moved away from the azeotropic composition, and therefore the copolymer became more heterogeneous. When the solvent was changed to acetone, which has a lower index of refraction compared with that of PMMA and is a nonsolvent for polystyrene, the slow mode was not diffusional, indicating association of the polymer chains in a poor solvent condition.[15]

Earlier we reported a DLS study of semidilute solutions of a random copolymer, poly(styrene-*co*-acrylonitrile) (SAN), with a high styrene content in toluene and fluorotoluene.[17] Chain-to-chain variations of the monomer composition and a random distribution of monomers along the chain make the copolymer solution heterogeneous on various length scales.[18] At concentrations higher than the overlap concentration, the DLS autocorrelation function exhibited a slow diffusion mode and an internal relaxation mode in addition to the fast cooperative diffusion mode. The slow mode slowed drastically with an increasing polymer concentration, indicating that it is the composition fluctuations (heterogeneity mode) made possible through self-diffusion of entangled chains. When the solvent was dioxane or *N*-methylpyrrolidone, in contrast, the copolymer exhibited only the fast mode at the same concentration. In homogeneous copolymer solutions in these nonselective solvents, the heterogeneity mode cannot be observed, because the self-diffusion does not lead to local refractive index fluctuations. In the study we also used a mixture of dioxane and acetonitrile (ACN) to prepare a semidilute solution of the copolymer. The solution in the mixture showed two diffusion modes, but the cooperative diffusion was much slower compared with the solution in the other solvents at the same concentration. We did not explore the concentration dependence in the ACN/dioxane mixture, because our primary interest was to find a relationship between the heterogeneity of the semidilute solutions and the performance of phase fluctuation chromatography in various solvents. The latter was developed to separate a copolymer by the chemical composition.[19−21]

The present contribution extends our preceding DLS study[17] of the copolymer solution to a wider range of concentrations in various mixing ratios of ACN and dioxane. We are especially interested in a near-Θ solvent condition. Dioxane is relatively nonselective to the two monomers of SAN compared with ACN that does not dissolve SAN fractions with a high styrene content. By changing the mixing ratio and the temperature of the solvent, we can provide the SAN fraction

10.1021/ma001646e CCC: $20.00
Published on Web 07/14/2001

Table 1. Refractive Index of Solvents

solvent	temp, °C	n_D	$n_F - n_C$	$n_{632.8}$
82.5/17.5	30.0	1.3509	0.005 54	1.3495
80/20	30.0	1.3523	0.005 56	1.3509
75/25	30.0	1.3556	0.006 50	1.3539
70/30	30.0	1.3590	0.005 59	1.3576
60/40	30.0	1.3663	0.006 56	1.3646
80/20	26.0	1.3542	0.005 57	1.3528
80/20	30.0	1.3523	0.005 56	1.3509
80/20	31.2	1.3515	0.006 48	1.3498
80/20	36.7	1.3490	0.005 54	1.3476
80/20	38.0	1.3477	0.005 52	1.3463
80/20	43.0	1.3455	0.006 56	1.3438
80/20	50.0	1.3430	0.005 50	1.3416

Table 2. Viscosity of Solvents

solvent	temp, °C	kinematic viscosity, cS	density, g/mL	η, cP
81/19	30.0	0.4578	0.8063	0.3691
75/25	30.0	0.4717	0.8221	0.3878
70/30	30.0	0.4824	0.8330	0.4018
60/40	30.0	0.5098	0.8557	0.4362
80/20	20.0	0.5022	0.8223	0.4130
80/20	33.0	0.4503	0.8085	0.3641
80/20	42.5	0.4209	0.7978	0.3358
80/20	51.5	0.3972	0.7877	0.3129

with a wide range of solvent quality. We use the same SAN fraction as the one used before. The solvent mixture with a high ACN content is good to the minority components of the copolymer, in contrast to toluene and fluorotoluene which are good to the majority components.

Experimental Section

Materials. The copolymer used in the present study is SAN20, poly(styrene-*co*-acrylonitrile), with a weight fraction of acrylonitrile at 20%, from Asahi Chemical, Japan. The molecular weight distribution was characterized in size exclusion chromatography with a refractive index detector. The weight-average and number-average molecular weights are 2.3×10^5 and 9.3×10^4, respectively, with reference to polystyrene standards.

Mixtures of acetonitrile (ACN) and 1,4-dioxane, both from Acros, at different mixing ratios were used as solvents for the copolymer. We denote by AD80/20 a mixture with 80% of ACN in weight, for instance.

Refractive Index Measurement. The refractive indices of the solvent mixtures were measured by using an Abbe refractometer (Edmond Scientific). The temperature was controlled by circulating water. The indices at 632.8 nm were calculated by linear interpolation from the reading of n_D (λ_D = 589.3 nm) and the dispersion $n_F - n_C$ ($\lambda_F - \lambda_C = -170.2$ nm). Table 1 lists n_D, $n_F - n_C$, and the calculated index at 632.8 nm for each of the solvent and temperature. Extrapolation was used to estimate the refractive index of AD50 which we did not measure. Note that the refractive indices of the solvents are much lower than those of the two components of the copolymer. The index is about 1.59 for polystyrene and 1.52 for polyacrylonitrile. Since the volume fraction of styrene is estimated to be 82% in the copolymer, the expected refractive index of SAN20 is around 1.58.

Viscosity Measurement. The kinematic viscosities of the solvent mixtures were measured at various temperatures by using an Ubbelohde viscometer (Cannon CUC-050) in a temperature-controlled water bath. The density of the solvent mixture was calculated by assuming an ideal mixture of the two pure solvents. Then, the viscosity was calculated as the product of the kinematic viscosity and the density. See Table 2 for the results. Interpolation and extrapolation were used to estimate the viscosity of the solvent mixtures used in DLS.

Dynamic Light Scattering Measurement. Dynamic light scattering (DLS) measurements were made by using a N4 Plus particle sizer (Beckman-Coulter) with a He−Ne laser (λ = 632.8 nm). The scattering angle is one of the six fixed angles between 15° and 90° (for air). The correlator in N4 Plus has 80 quasi-logarithmically spaced delay channels, equivalent to 3072 linearly spaced channels. The temperature of the cell can be controlled in the range between 0 and 90 °C. The solution was filtered through a PTFE membrane filter with 0.2 μm pore size (Millipore) into a dust-free fluorometer cell (10 × 10 mm; UVONIC type 23). Use of the square cuvette and fixed-angle detection makes the scattering angle θ slightly dependent on the refractive index of the solvent except for $\theta = 90°$. The angle θ calculated from the ray optics is used in the system. The N4 Plus system is not designed for the static light scattering measurement in which we would obtain R_g, the root-mean-square radius of gyration of the polymer.

The baseline-subtracted, normalized autocorrelation function $g_2(t)$ of the scattering intensity was obtained as a function of the delay time t. The absolute value of the electric-field autocorrelation function $g_1(t)$ (after baseline subtraction and normalization) is related to $g_2(t)$ by $g_2(t) = [g_1(t)]^2$. A CONTIN program[22] analyzes $g_1(t)$ to obtain the spectrum $G_D(D)$ of the diffusion coefficient D by inverse-Laplace transform:

$$g_1(t) = \int G_D(D) \exp(-Dk^2t)\, dD = \int DG_D(D) \exp(-Dk^2t)\, d \ln D \quad (1)$$

where the scattering vector k is related to the scattering angle θ by $k = (4\pi n/\lambda) \sin(\theta/2)$, with n being the refractive index of the solvent. The range of D that can be analyzed in one measurement is about 3 decades. The particle sizing system assumes that all of the decay in $g_1(t)$ is due to the center of mass diffusion of independent spherical suspensions of different sizes. It is straightforward to convert $G_D(D)$ into a distribution $G_d(d_{app})$ of the apparent diameter d_{app} of the "particle". Note that $G_d(d_{app})$ is weighted by the scattering intensity of each particle. The Stokes−Einstein relationship gives d_{app} as

$$d_{app} = \frac{k_B T}{3\pi\eta D} \quad (2)$$

where k_BT is the thermal energy and η is the solvent viscosity. In the dilute solution limit and when θ is sufficiently small, d_{app} obtained in this way is twice as large as the hydrodynamic radius. A peak in the size distribution does not necessarily mean that the particles of d_{app} are present in the solution, however. It can be a center-of-mass diffusion slowed by entanglement, for instance. It is customary to display $d_{app}G_d(d_{app})$ in a logarithmic scale of d_{app}. Representing the dynamic spectrum in d_{app} is useful to compare the spectra obtained in different solvents or at different temperatures.

Results

1. Solubility. Figure 1 shows the appearance of the copolymer solution at 30 °C for solutions of various polymer concentrations in solvents of different ACN contents. The solution was clear in the solvent mixture up to 81% in ACN regardless of the polymer concentration c in the range studied. When the mixture contained ACN at 82% or higher, the solution was slightly whitish, again regardless of c. The hazy solution did not separate into different macroscopic phases for at least several months. The following DLS studies were conducted for clear solutions only.

2. Dynamic Light Scattering. Figure 2a shows the autocorrelation function $g_2(t)$ as a function of the delay time t measured at $\theta = 63.0°$ for solutions of SAN20 in AD80/20 at several selected concentrations at 30 °C. At low concentrations, $g_2(t)$ is nearly single-exponential and shifts to a longer delay time as c increases to 0.0884 g/mL. At higher concentrations, $g_2(t)$ has a long-time tail

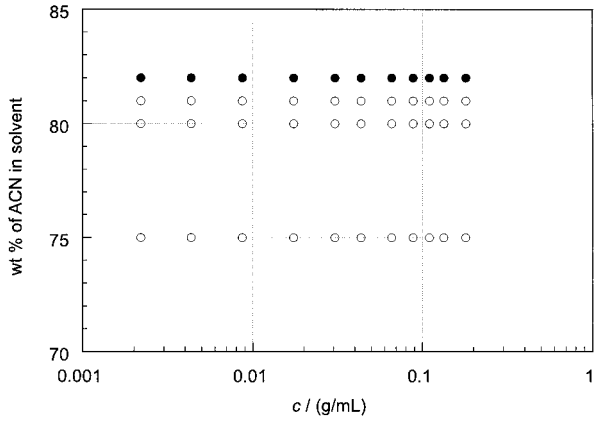

Figure 1. Appearance of solutions of SAN20 in acetonitrile/dioxane mixtures of various mixing ratios at different concentrations. Open and closed circles denote clear and cloudy solutions, respectively. The temperature is 30 °C.

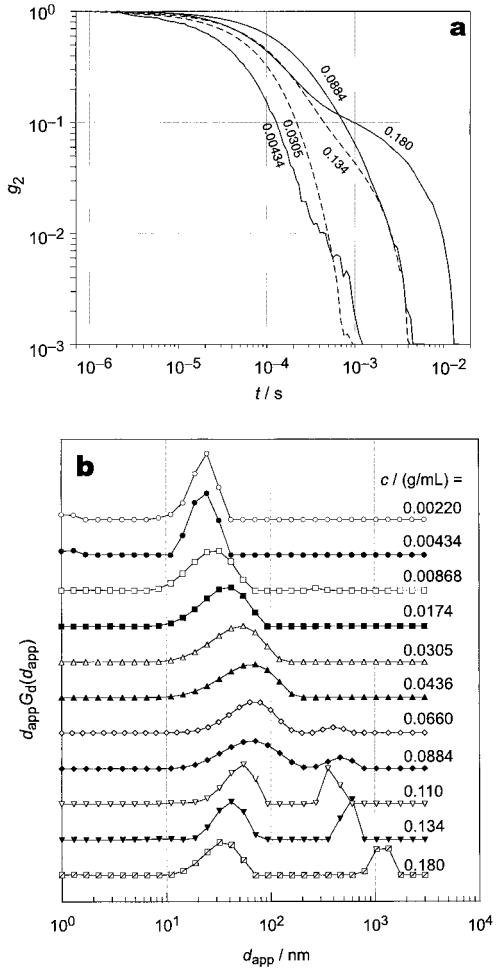

Figure 2. DLS results of SAN20 solutions in AD80/20 measured at $\theta = 63.0°$ in various concentrations at 30 °C. (a) Baseline-subtracted, normalized autocorrelation functions $g_2(t)$ plotted as a function of delay time t. (b) Distribution ($d_{app}G_d(d_{app})$; normalized) of the apparent diameter d_{app}. The polymer concentration is indicated adjacent to each curve.

(slow mode) that increases its height and becomes slower with an increasing c, whereas the main relaxation moves slightly in the opposite direction.

The distribution G_d of the apparent diameter d_{app} evaluated from $g_2(t)$ is shown in Figure 2b for different concentrations including those shown in Figure 2a. Small peaks at the left end of the distribution for $c =$ 0.0220 and 0.0434 g/mL are artifacts due to short delay times and weak scattering intensities. Apparently, the molecular weight distribution of the copolymer did not cause a serious broadening of the diameter distribution. As c increases, the peak shifts to a greater diameter with a concomitant broadening. At $c = 0.0660$ g/mL, a second peak (slow mode) appears at about 400 nm. As c further increases, the first peak (fast mode) shifts to a smaller diameter and narrows. The slow mode moves to a greater diameter.

For the same set of solutions, $g_2(t)$ was also obtained at 25, 40, and 50 °C in AD80/20. The trend in $g_2(t)$ and $G_d(d_{app})$ with an increasing c was close to the trend at 30 °C. The distribution was broader in the middle range of concentrations studied. At higher temperatures, the shift in the peak position of the fast mode was smaller, and the slow mode had a smaller d_{app}. The percentage of the slow mode in G_d was higher at a higher concentration and at a lower temperature but was capped to about 35%.

When the temperature was held at 30 °C but the solvent composition was changed, the pattern was drastically different. We studied the concentration dependence for 75, 70, 50, and 0% ACN in the solvent. Figure 3 shows the plots of $G_d(d_{app})$ with (a) 70% and (b) 50% of ACN, measured at $\theta = 63.1°$ and 63.4°, respectively. Compared with AD80/20, AD75/25 (not shown) had a smaller shift in the peak position of the fast mode with c and a smaller particle size and a lower height in the slow mode. The pattern of the change was close to that of AD80/20 at 40 and 50 °C. When the ACN content decreased to 70%, the peak position barely changed with concentration until it started to move to a smaller d_{app} at about 0.03 g/mL. The slow mode had only a small amplitude when it was observed at the two highest concentrations. When the ACN content further decreased to 50%, the fast mode moved to a smaller d_{app} monotonically as in pure dioxane (not shown). The relative amplitude of the slow mode was even smaller.

Figure 4 compares $G_d(d_{app})$ in various contents of ACN in the solvent, but at the same copolymer concentration of 0.0884 g/mL, $\theta \cong 63°$, and 30 °C. With an increasing ACN content, the fast mode becomes slower. In contrast, d_{app} of the slow mode was almost independent of the solvent composition when it was observed in solvents with a 70% or higher ACN content. The amplitude of the slow mode relative to the fast mode increased with the ACN content. The trend was similar at other concentrations when the two modes were observed.

The software in N4 Plus calculates the average of d_{app} for each of the peaks in $G_d(d_{app})$. In the following we use d_{app} to denote its average. All of the dynamic modes observed in $g_2(t)$ were diffusional. Table 3 lists typical results of d_{app} obtained for the solutions in AD80/20, 40 °C at 0.00434 and 0.134 g/mL. The values of d_{app} are not much different from angle to angle for both fast and slow modes and are within errors of measurement and spectral analysis.

Unlike in toluene and fluorotoluene,[17] an internal relaxation mode with the relaxation time independent of θ was either not observed or embedded in another mode in the ACN/dioxane mixtures. At $\theta \cong 63°$ and $c =$ 0.11 g/mL, d_{app} for the internal mode showed up at around 100 nm in the two solvents.

Figure 5 shows d_{app} for the fast and slow modes as a function of polymer concentration c measured at differ-

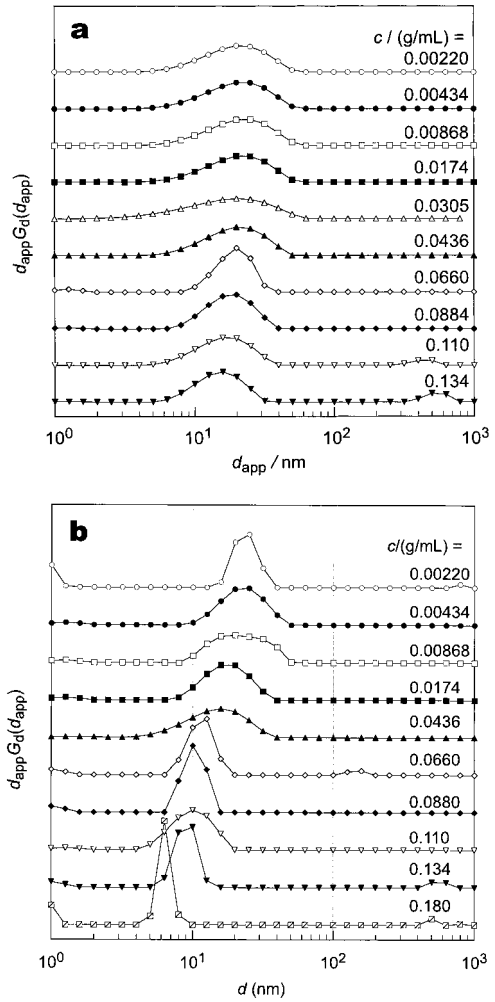

Figure 3. Distribution of the apparent diameter d_{app} in solution of SAN20 in (a) AD70/30 and (b) AD50/50, measured at 30 °C. The scattering angle is (a) 63.1° and (b) 63.4°. The polymer concentration is indicated adjacent to each curve.

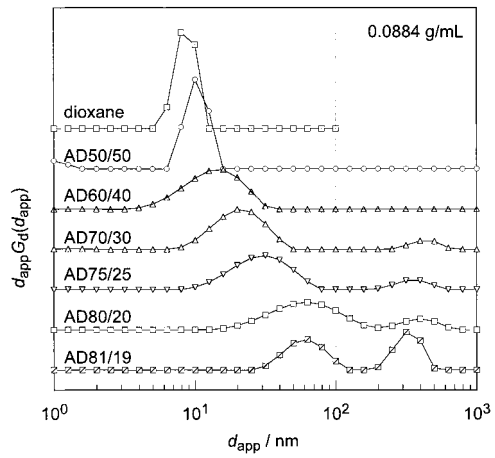

Figure 4. Distribution of the apparent diameter d_{app} in a 0.0884 g/mL solution of SAN20 in various contents of ACN in the solvent, measured at 30 °C and $\theta \cong 63°$.

ent temperatures for solution in AD80/20, $\theta \cong 63°$. When G_d has a single mode, it is plotted as the fast mode. For all the temperatures studied, d_{app} of the fast mode initially increases with c, followed by a decrease. The concentration at which d_{app} of the fast mode maximizes is almost the same for different temperatures. At higher concentrations, d_{app} decreases in proportion to c^{-1}. At

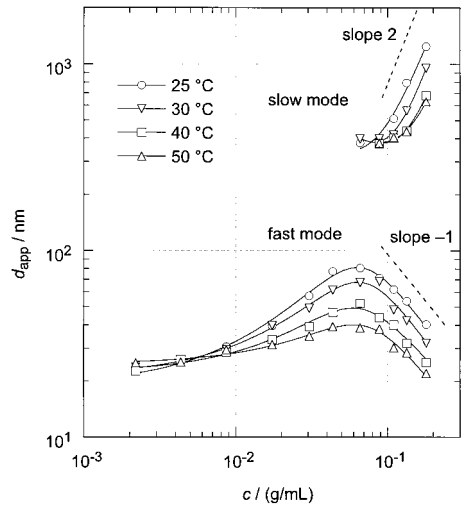

Figure 5. Average of the apparent diameter d_{app} for the fast and slow modes in solutions of SAN20 in AD80/20 measured at different temperatures at $\theta \cong 63°$, plotted as a function of polymer concentration c. The temperature is indicated in the legend. The dashed lines represent slopes of 2 and −1.

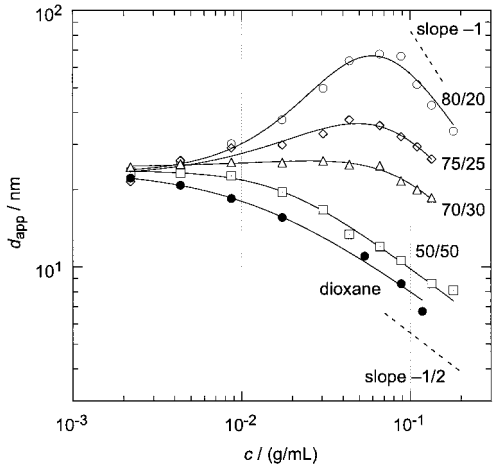

Figure 6. Average of the apparent diameter d_{app} for the fast mode in solutions of SAN20 in ACN/dioxane mixtures of various ACN contents measured at 30 °C and $\theta \cong 63°$, plotted as a function of polymer concentration c. The ACN content is indicated adjacent to each curve. The dashed lines represent slopes of −1 and $-1/2$.

Table 3. Results for d_{app}/nm at Different Scattering Angles

		c = 0.134 g/mL	
θ (deg)	c = 0.0434 g/mL	fast mode	slow mode
15.4	25.3	31.5	398
22.6	26.8	33.3	392
29.6	28.6	37.0	445
63.1	29.7	32.8	417
90.0	23.3	33.3	469

the concentration where d_{app} maximizes, the slow mode starts to appear. The latter increases its d_{app} in proportion to c^2 near the high end of the concentration range measured. At $c > 0.005$ g/mL, d_{app} of the fast mode is greater; i.e., the fast mode is slower, at a lower temperature compared at the same concentration. The same applies to the slow mode. At $c < 0.005$ g/mL, this trend is reversed.

The pattern of the change in d_{app} with concentration becomes different when the ACN content decreases in the solvent. Figure 6 shows the change of d_{app} for the

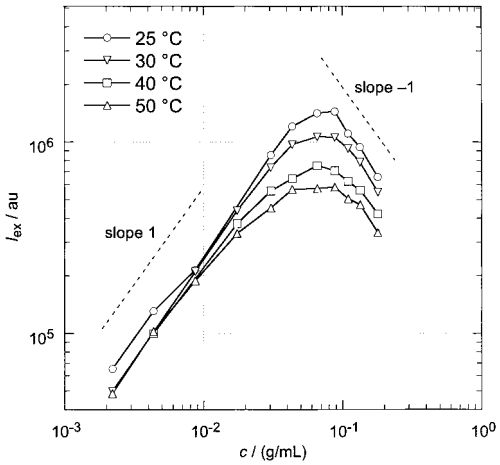

Figure 7. Excess scattering intensity I_{ex} (photon counts) at $\theta \cong 63°$ from a solution of SAN20 in AD80/20 at different temperatures, plotted as a function of polymer concentration c. The temperature is indicated in the legend. The dashed lines represent slopes of 1 and −1.

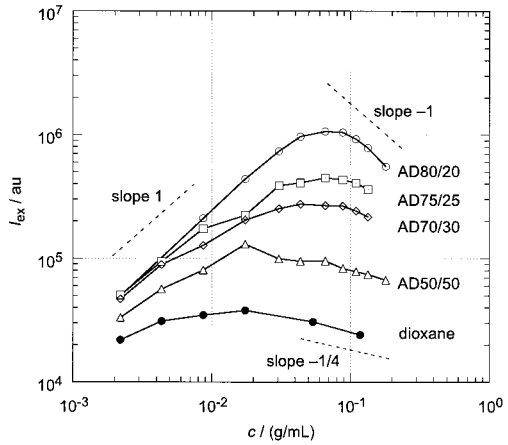

Figure 8. Excess scattering intensity I_{ex} (photon counts) at $\theta \cong 63°$ for a solution of SAN20 in ACN/dioxane mixtures of various ACN contents measured at 30 °C, plotted as a function of polymer concentration c. The ACN content is indicated adjacent to each curve. The dashed lines represent slopes of 1, −1, and $-1/4$.

fast mode at 30 °C. The slow mode is not displayed here. The slow mode observed in AD75/25 and AD70/30 at $c > 0.06$ g/mL has d_{app} that increased from 350 to 500 nm with an increasing c. Compared at the same concentration, the fast mode is faster when the ACN content is lower. This trend persists in the entire range of concentrations measured except for the lowest concentration where comparison is difficult. The fast mode in AD70/30 has nearly a flat d_{app} until it starts to decrease at around 0.06 g/mL. At a higher ACN content in the solvent, there is a peak in d_{app}. The AD75/25 has the peak at a lower concentration compared with AD80/20. The dependence of d_{app} on c at $c > 0.08$ g/mL is different from solvent to solvent. The slope for the dependence changes from −1 in AD80/20 to $-1/2$ in AD50/50 and dioxane.

3. Scattering Intensity. The excess scattering intensity I_{ex} of a solution with reference to the solvent is obtained as the difference in the average photon counts per second between the solution and the solvent. Figure 7 shows I_{ex} at $\theta \cong 63°$ as a function of c for the solutions in AD80/20 at different temperatures. At low concentrations, I_{ex} was almost proportional to c for all the temperatures, a reasonable result. The intensity peaks at $c_{peak} \cong 0.08$ g/mL, close to the concentration at which d_{app} of the fast mode maximizes and the slow mode appears. The peak intensity is lower at a higher temperature. At $c > c_{peak}$, I_{ex} decreases approximately in proportion to c^{-1}. The concentration dependence was the same at other scattering angles (not shown).

Figure 8 shows I_{ex} at $\theta \cong 63°$ as a function of c for the solutions in different contents of ACN measured at 30 °C. At low concentrations, I_{ex} appears to be nearly proportional to c in all ACN contents, although in dioxane there is no linear range; We could not lower the concentration further without compromising the accuracy. Surprisingly I_{ex} from the solutions with high ACN contents, especially in AD80/20, exhibits a good linearity to a high concentration on the double-logarithmic scale. The peak intensity decreases and c_{peak} shifts to a lower concentration as the ACN content decreases in the solvent. The dependence of I_{ex} on c at higher concentrations shows a crossover from c^{-1} in AD80/20 to $c^{-1/4}$ in AD50/50 and dioxane.

Table 4. Fitting Parameters

solvent	temp, °C	d_0, nm	k_d, mL/g	$2A_2M$, mL/g	k_f, mL/g
AD80/20	25.0	20.6	1050	−3	1050
AD80/20	30.0	22.1	907	0.25	907
AD80/20	40.0	23.1	546	11	557
AD80/20	50.0	25.0	336	21	356
AD72/25	30.0	24.3	319	37	356
AD70/30	30.0	23.8	8	69	78
AD50/50	30.0	25.1	−249	222	−27
dioxane	30.0	23.4	−565	568	3

Discussion

We discuss the results in two parts. The first is for the concentration range in which only one mode was observed in $g_2(t)$ in the high ACN contents. The second is for the range in which two modes were observed in the solvents. The single mode−fast mode is the mutual diffusion that changes over to the cooperative diffusion as the chains overlap, as discussed below. The slow mode observed in highly selective solvents is due to heterogeneity of the copolymer solution. Between the two parts, we briefly discuss about the osmotic modulus of the solutions in the whole range of concentrations.

1. Single-Mode Concentration Range. At low concentrations we can approximate d_{app} by $d_0(1 + k_d c)$. In fact, the range in which this linear fitting (not shown) is good in Figures 5 and 6 extends to 0.0434 g/mL except for dioxane at 30 °C. In the latter, the limited number of data points in the linear range makes the estimates of d_0 and k_d less reliable compared with those of other solvents. Note that this k_d is the negative of the linear coefficient in the concentration dependence of the diffusion coefficient. Table 4 lists k_d and d_0 obtained by the fitting. Likewise, c/I_{ex} can be approximated by constant × $(1 + 2A_2Mc + R_g^2k^2/3)$ in the same concentration range, where A_2 is the osmotic second virial coefficient, M the molecular weight, and R_g^2 the mean-square radius of gyration. We used the relationship[23] $R_g = 1.5(d_0/2)$ to estimate $2A_2M$ in the fitting. It is known[24] that $k_d = k_f - 2A_2M$, where k_f is the linear concentration coefficient of the friction against the chain's motion. The backflow correction is small (∼1 mL/g) and neglected here. Table 4 lists $2A_2M$ and k_f also. Again, the estimates for dioxane are less reliable. Parts a and b of Figure 9 show how k_d, $2A_2M$, and k_f change with temperature in AD80/20 and with the ACN content

Table 5. Scattering Intensity in Dilute Solutions

solvent	n_s	$n_p - n_s$	$H' = [n_s(n_p - n_s)]^2$	I_{ex}/c	$I_{ex}/(cH')$
AD80/20	1.3509	0.226	0.0933	2.26E+07[a]	2.42E+08
AD75/25	1.3539	0.223	0.0912	2.30E+07	2.52E+08
AD70/30	1.3576	0.219	0.0887	2.14E+07	2.41E+08
AD50/50	1.3646	0.212	0.0840	1.51E+07	1.80E+08
dioxane	1.4170	0.160	0.0514	9.95E+06	1.94E+08

[a] Read as 2.26×10^7.

at 30 °C, respectively. At 30 °C (part b), the negative k_d at low contents of ACN increases with an increasing ACN content and becomes near zero in AD70/30, followed by a sharp increase as the ACN content further increases. In the whole range of the ACN contents measured, $2A_2M$ decreases linearly with the ACN content and becomes near zero at 80% of ACN, indicating that the solvent is good to the copolymer when the ACN content is less than 50% but near Θ when the content is more than 70%. The sharp increase in k_d toward the high end of the ACN content is therefore due to the sharp increase in k_f. The latter remains nearly unchanged and small when the solvent is good. In the temperature dependence in AD80/20 (part a), all of k_d, $2A_2M$, and k_f changes linearly with temperature in the range measured. The second virial coefficient becomes zero at $T \cong 28.8$ °C. At all temperatures, k_f is a dominant term in k_d. It is now clear that AD80/20 is near Θ, especially at 30 °C. At 25 °C it is poorer than the Θ solvent is.

The fitting parameters for AD80/20 at 50 °C are close to those obtained for AD75/25 at 30 °C. The higher temperature is effective in providing an environment of a better solvent in the same way as increasing the percentage of the nonselective solvent. This similarity is also manifested in the other properties as shown below.

A similar change in k_d was observed in solutions of polystyrene in cyclohexane,[25,26] decahydronaphthalene,[24] and poly(α-methylstyrene) in cyclohexane[27] and ascribed to the change in k_f. A uniform distribution of the chains in the solution would not make k_f so large, however. It is known[28] that polymer chains in a Θ to poor solvent tend to form dynamic clusters at concentrations above the overlap concentration of the swollen chains. Local crowding of the chains will hinder the motion of the chain, thereby increasing k_f dramatically.

There is no hint of chain aggregation in the low concentration limit, however. We rather see a systematic decrease of d_0 (Table 4) in AD80/20 as the temperature drops, indicating that each chain contracts more as the solvent turns poorer. The change of d_0 with the ACN content at 30 °C was not as systematic, especially for dioxane. We had expected that d_0 would increase with a decreasing ACN content. This mismatch is probably due to the error in the estimate of d_0 in dioxane.

The state of molecular dispersion at low concentrations is corroborated by the following fact. At low concentrations, I_{ex} is proportional to $(n_s\, dn/dc)^2 c$, where n_s is the refractive index of the solvent and dn/dc is the differential refractive index of the polymer in the solvent. For a rough estimate, we assume that dn/dc is proportional to $n_p - n_s$, where $n_p \cong 1.58$ is the refractive index of SAN20. Table 5 lists n_s, $n_p - n_s$, $H' \equiv [n_s(n_p - n_s)]^2$, I_{ex}/c, and $I_{ex}/(cH')$ evaluated for the near-linear range of the plots in Figure 8. If the polymer chains are molecularly dispersed and each chain moves independently, then $I_{ex}/(cH')$ should be the same within experimental errors. We find that it is the case. The relatively small values of $I_{ex}/(cH')$ in AD50/50 and dioxane are again ascribed to experimental errors in the estimate of I_{ex} that depend on the small difference in the scattering intensity between the solution and the solvent. In Figure 7, the plots for different temperatures nearly overlap at low concentrations. Since the refractive indices depend on the temperature only weakly, this result confirms the same state of the chains as the temperature changes and therefore the solvents quality changes.

The overlap concentration $c^* = (M/N_A)(2^{1/2}R_g)^{-3}$ is estimated to be 0.020−0.040 g/mL for polymer chains with $d_0 = 25-21$ nm. For dioxane and AD50/50 which have a large positive A_2, I_{ex} starts to deviate from the linear relationship at concentrations below c^* in Figure 8. As soon as the swollen chains start to overlap with neighboring chains, the mutual diffusion gains more of the characteristics of the cooperative diffusion. A decrease in the number of monomers in the shrinking volume of correlated density fluctuations leads to the downward deviation of I_{ex}.

Compared with dioxane and AD50/50, the other solvents have a more extended concentration range in which I_{ex} is nearly proportional to c and a single mode is observed. In particular, in AD80/20 at 25 °C the range extends beyond c^*. There poorer solvents must have a mechanism to prevent I_{ex} from deviating downward with an increasing c. We ascribe it again to the chain clustering. If the polymer chains form clusters, I_{ex} will increase by a factor equal to the number of chains in each cluster compared with the molecularly dispersed solution without chain overlap. All of the results obtained in the single-mode range point to the presence of clusters in the near-Θ solvents and indicate that the number of chains per cluster increases with an increasing c, thereby minimizing or preventing the downward deviation of I_{ex}. This tendency is stronger for a solvent with a higher ACN content and at a lower temperature, thus approaching the poor solvent condition.

In contrast to ACN−dioxane mixtures with a high ACN content, I_{ex} started to deviate from a linear relationship at around c^* in toluene and fluorotoluene[17] just as in dioxane. The slow mode appeared at around c^* in toluene and fluorotoluene.

We believe the broadening in the relaxation spectrum in the middle concentration range is not due to an artifact introduced by CONTIN. The broadening is rather related to the onset of entanglement. Solutions at around c^* are more heterogeneous than those of other concentrations, resulting in a broader range of relaxation times.

2. Osmotic Modulus. The excess scattering intensity data obtained at low angles allow us to estimate the osmotic modulus $\partial\Pi/\partial c$ because

$$\frac{\partial(\Pi/RT)}{\partial c} \propto \frac{c}{I_{ex}} H' \tag{3}$$

where R is the gas constant. When cH'/I_{ex} is plotted as a function of c (not shown), the data points are scattered. Using the reduced concentration A_2Mc for the abscissa is effective in removing the scattered nature as shown in Figure 10. AD80/20, 25 °C is not included because its A_2 is negative. At low concentrations, the data points appear to lie on a single horizontal line (Table 5). With

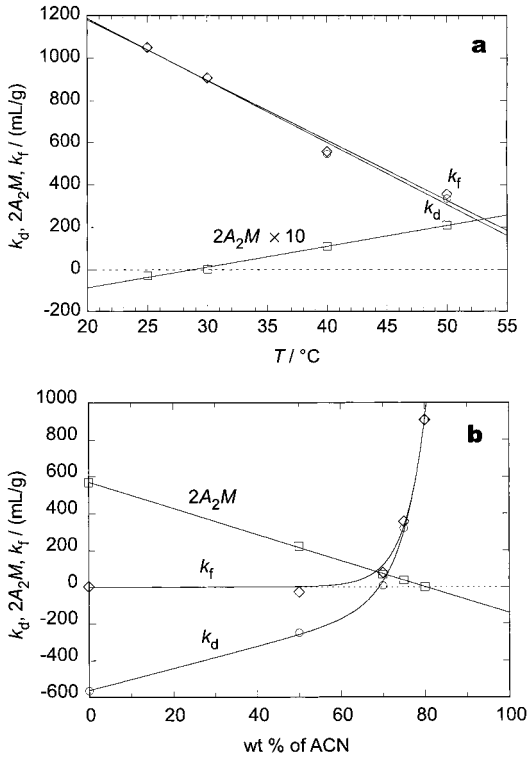

Figure 9. Concentration coefficient k_d of d_{app}, the osmotic second virial coefficient times the molecular weight, $2A_2M$, and the concentration coefficient k_f of the friction coefficient are shown in (a) AD80/20 at various temperatures and (b) various ACN/dioxane mixtures at 30 °C. In (a), $2A_2M$ is multiplied by 10. The lines are for the eye guide.

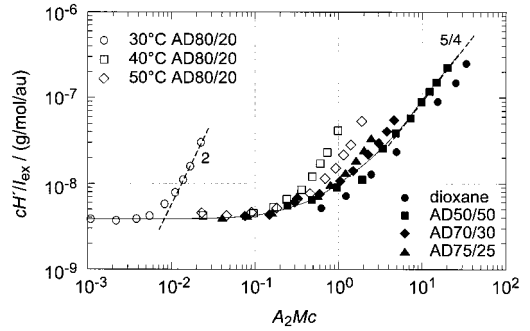

Figure 10. Reciprocal of the reduced scattering intensity, cH'/I_{ex}, plotted as a function of the reduced concentration A_2Mc. The data for AD80/20, 25 °C are not included. The solid line is an expected master curve. The slopes of the dashed lines are $^5/_4$ and 2.

an increasing c, the difference in the solvent quality becomes apparent. When the solvent is sufficiently good, the data points appear to approach a master curve shown by a solid line. This master curve is close to the one obtained for solutions of polystyrene in toluene.[29] The data points for dioxane again deviate probably because of the overestimated A_2. The slope in the semidilute range shows a crossover from $^5/_4$ in AD50/50, 30 °C to 2 in AD80/20, 30 °C as the solvent becomes poorer, in agreement with the scaling theory[30] for semidilute solutions in a good solvent and a Θ solvent, respectively.

3. Two-Mode Concentration Range. a. Fast Mode. We apply the blob picture to the fast mode. The blob picture[30] assumes that the solution consists of blobs of length l (≅ correlation length), each consisting of g monomers. In the blob, the partial chain follows the

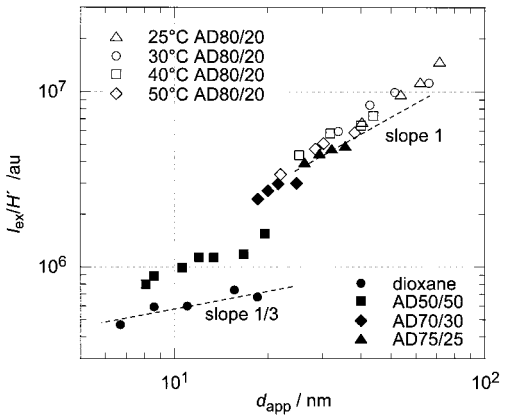

Figure 11. Reduced scattering intensity, I_{ex}/H', plotted as a function of d_{app} for the data obtained in the two-mode range or above c^*.

statistics of an isolated chain. Therefore, $ag^\nu \cong l$ ($\nu = {}^1/_2$ in the Θ solvent and $\cong {}^3/_5$ in the good solvent). The whole solution is packed with blobs of volume l^3. Assuming that each blob scatters photons independently and the photons scattered by the g monomers in the blob are coherent, we obtain $I_{ex} \propto l^{-3}g^2 \propto l^{-3+2/\nu}$. In the good solvent, $I_{ex} \propto l^{1/3}$. In the Θ solvent, $I_{ex} \propto l$. What is measured as d_{app} in DLS represents l. Figure 11 shows a plot of I_{ex}/H' as a function of d_{app}. Only the data in the two-mode range or above c^* are shown. The slope for the data points shows a crossover from $^1/_3$ in dioxane to 1 in AD80/20 as the solvent becomes poorer, supporting the blob picture. In this figure, the shift in the data points from dioxane to AD70/30 is remarkable, compared with the nearly overlapping data points in Figure 10 for the same solvents. A modestly poor solvent is sufficient to make the dynamics greatly different. Once the solvent is near Θ, the data points almost overlap on top of the others, but the solvent-to-solvent variation still exists.

The blob picture is also evident in the plots of I_{ex} and d_{app} as a function of c. In the good solvent ($I_{ex} \propto l^{1/3}$ and $l \cong d_{app} \propto c^{-3/4}$), $I_{ex} \propto c^{-1/4}$. In the Θ solvent ($I_{ex} \propto l$ and $l \propto c^{-1}$),[31] $I_{ex} \propto c^{-1}$. From the dependences of d_{app} of the fast mode and I_{ex} on c in the relevant concentration ranges in Figures 5−8, we can ascribe the fast mode to the cooperative diffusion—fluctuations of the total monomer density in a blob. From these results alone, we can conclude that dioxane and AD50/50 are good solvents for SAN20, adding ACN makes the solvent poorer, AD80/20 is a near-Θ solvent at 25−30 °C, and increasing the temperature makes the solvent better. These findings are in agreement with the change in A_2 shown in Figure 9a,b.

In the semidilute solutions of the copolymer in toluene and fluorotoluene, $I_{ex} \propto c^{-1/4}$ and $d_{app} \propto c^{-1/3}$. The former indicated that toluene and fluorotoluene are good solvents, but the exponent of $-{}^1/_3$, much smaller than $-{}^3/_4$ in absolute value, was not explained.[17]

b. Slow Mode. In contrast to the ubiquity of the fast mode, the slow mode is observed only when the solvent is near Θ. The relative amplitude of the slow mode in $g_2(t)$ increases as the solvent becomes poorer, thereby making the solution more heterogeneous.

We speculate that the slow mode is due to the center-of-mass diffusion of the copolymer chain. Dependence of the relative height of the slow mode on the scattering angle, the concentration, and the solvent composition was not as clear as that of d_{app}. We refrain from further

discussion here. For a more definitive statement, DLS measurements need to conducted for more concentrated solutions. Further studies are needed experimentally and theoretically.

c. Statistics of Partial Chains in the Blobs. Having seen a crossover from good to Θ condition by changing the solvent composition and the temperature, we are now tempted to examine the statistics of partial chains in the blobs based on the light scattering data alone. Here we preclude any prior knowledge regarding the statistics of the partial chain in each blob. We rather assume that the whole volume of the semidilute solution consists of blobs without voids, the blobs behave as if they were independent scatterers of size d_{app}, and the g monomers in the blob scatter the photons coherently. Our procedure is similar to the one employed by Hamada et al. in their small-angle X-ray scattering studies on semidilute solutions of polystyrene in toluene[33] and cyclohexane.[34]

The scattering intensity of the semidilute solution is proportional to $d_{app}^{-3}g^2$, just as it is proportional to $(c_1N_A/M)N^2$ in the dilute solution at concentration c_1, where c_1N_A/M is the number of polymer chains in unit volume (N_A is Avogadro's number), and N is the number of monomers in the chain. Thus,

$$\frac{I_d(c_1)}{(c_1N_A/M)N^2} = \frac{I_{sd}}{d_{app}^{-3}g^2} \tag{4}$$

where $I_d(c_1)$ is I_{ex} of the dilute solution at c_1, and I_{sd} is I_{ex} of the semidilute solution. $I_d(c_1)/c_1$ is listed in Table 5. Rearrangement gives

$$g/N = \left[\frac{I_{sd}d_{app}^{3}}{[I_d(c_1)/c_1](M/N_A)}\right]^{1/2} \tag{5}$$

Measuring I_{sd} and I_d at the same temperature and for the same set of polymer and solvent eliminates the difference in the prefactor to the scattering intensities in eq 5 between different solvents and temperatures, as long as the relationship between g/N and d_{app} is the same. In fact, eq 5 eliminates the difference in the polymer as well. In Figure 12a, we plot d_{app} as a function of g/N thus estimated for all the data shown in Figures 6 and 8 in the two-mode range or above c^*. We used for M the weight-average molecular weight estimated in size exclusion chromatography. The error in the estimate is common to all solvents. Fitting the data for each solvent by $d_{app} \sim (g/N)^{\nu}$ gives the exponent $\nu = 0.57$, 0.56, 0.54, 0.54, and 0.51 for dioxane, AD50/50, AD70/30, AD75/25, and AD80/20, respectively, at 30 °C. The partial chain in the blob follows the conformation of swollen chains in dioxane. As the ACN content increases, the conformation approaches that of the Θ chain. The symbols in different solvents do not follow a master curve; d_{app} in a better solvent is greater compared at the same d_{app}. The partial chain swells more in the better solvent. Figure 12b is a similar plot for AD80/20 at different temperatures. All the data points fall closely on a master curve with a slope of $^1/_2$, but fitting the data of each temperature separately gives $\nu = 0.46$, 0.51, 0.51, and 0.50 at 25, 30, 40, and 50 °C, respectively. Apparently at 25 °C the chains contract more than the Θ chains do, in agreement with the change in A_2 with temperature.

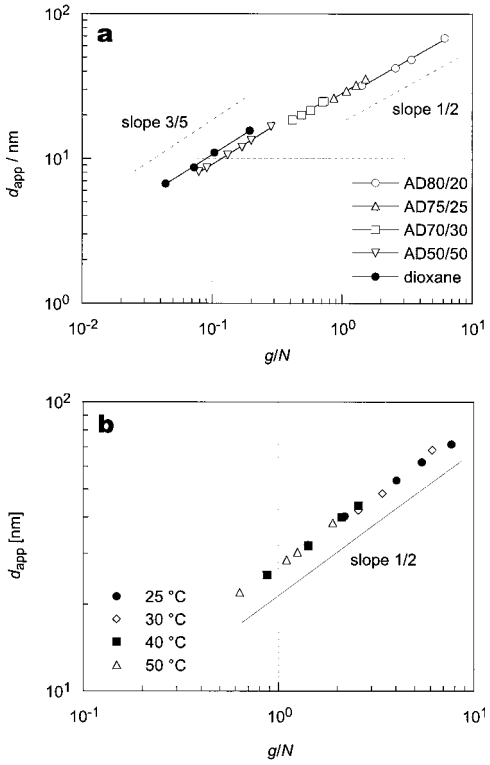

Figure 12. Relationship between the apparent diameter d_{app} for the fast mode (blob size) in semidilute solutions and the number of monomers g in each blob reduced by the number N in the whole chain. (a) Different solvent compositions at 30 °C. The dashed lines represent slopes of $^3/_5$ and $^1/_2$. (b) Different temperatures in AD80/20. A line with a slope of $^1/_2$ is shown.

Note that g/N is greater than unity for most of the data in Figure 12b and some in Figure 12a. Then, what is plotted is not for a partial chain, but for a superchain—a cluster. The values of the greatest g/N are 7.7, 6.2, 2.9, and 1.9 at 25, 30, 40, and 50 °C in AD80/20, respectively, reached at $c = 0.0884$ g/mL. At 25 °C, the cluster takes a conformation of a Θ chain whose contour is 8 times as long.

The superchain is still too short to make I_{ex} depend visibly on the scattering angle. In our measurements, $I_{ex}(\theta \cong 15°)/I_{ex}(\theta = 90°)$ was independent of the concentration (not shown) within experimental errors. In AD80/20 at 30 °C, $c = 0.0848$ g/mL which showed the Θ exponent, i.e., $d_{app} \sim (g/N)^{1/2}$, for instance, $kR_g = 0.97$ at $\theta = 90°$, and therefore $(kR_g)^2/3 = 0.31$. This kR_g is insufficient to decrease I_{ex} appreciably on the logarithmic scale.

We do not see a tendency of a changing slope as g/N decreases in Figure 12b. The environment for the polymer is held unchanged. A sharp drop in d_{app} of the fast mode and I_{ex} with an increasing c in Figures 6 and 8 have not resulted from decreasing polymer−solvent interactions as the volume fraction of the polymer increases. The clustered chains overlap to exhibit the cooperative diffusion mode and the heterogeneous mode in the semidilute solutions. It is not that the clusters are disintegrated before the chain overlap.

Conclusions

We used DLS to study dynamics of dilute and semidilute solutions of a random copolymer consisting of styrene and acrylonitrile. Mixtures of acetonitrile and dioxane in varying mixing ratios were used to provide the polymer with an environment that ranges from a

good solvent to a near-Θ solvent. Cooperative diffusion of swollen chains changed over to the cooperative diffusion of the Θ chains plus a slow heterogeneous diffusion mode as the solvent quality became poorer. Indication of clustering was also observed in the latter solvent.

Together with our preceding results in toluene and fluorotoluene, we have shown that a variety of patterns in the concentration dependence of the light scattering intensity and the diffusion coefficient can be observed for the random copolymer by changing the solvent condition. We have not invoked any optical masking techniques so far.

Further DLS studies on the semidilute copolymer solutions will elucidate the nature of the dynamics. The systems to be studied will include (1) the same copolymer fraction in mixtures of a nonselective solvent and a solvent that selectively dissolves polystyrene, (2) other fractions of SAN in dioxane/ACN mixtures, and (3) other random copolymers in appropriate solvents. Frustration in a system that tries to separate into different phases but fails to do so because of covalent bonding may lead to interesting phenomena, just as the diblock copolymer solutions do. The randomness of the monomer sequence positions the random copolymer between the homopolymer and the diblock copolymer in terms of solution thermodynamics. Unlike the latter, we can choose a variety of solvents and therefore change the interactions of the solvent to the two constituents of the copolymer without formation of micelles.

Acknowledgment. We acknowledge support from Division of Materials Research at National Science Foundation. We also appreciate the loan of N4 Plus from Beckman-Coulter.

References and Notes

(1) Brown, W.; Nicolai, T. In *Dynamic Light Scattering*; Brown, W., Ed.; Oxford University Press: New York, 1993.
(2) Jian, T.; Anastasiadis, S. H.; Semenov, A. N.; Fytas, G.; Adachi, K.; Kotaka, T. *Macromolecules* **1994**, *27*, 4762.
(3) Pan, C.; Maurer, W.; Liu, Z.; Lodge, T. P.; Stepanek, P.; von Meerwall, E. D.; Watanabe, H. *Macromolecules* **1995**, *28*, 1643.
(4) Liu, Z.; Pan, C.; Lodge, T. P.; Stepanek, P. *Macromolecules* **1995**, *28*, 3221.
(5) Semenov, A. N.; Anastasiadis, S. H.; Boudenne, N.; Fytas, G.; Xenidou, M.; Hadjichristidis, N. *Macromolecules* **1997**, *30*, 6280.
(6) Akcasu, A. Z.; Benmouna, M.; Benoit, H. *Polymer* **1986**, *27*, 1935.
(7) Benmouna, M.; Benoit, H.; Duval, M.; Akcasu, A. Z. *Macromolecules* **1987**, *20*, 1107.
(8) Borsali, R.; Duval, M.; Benoit, H.; Benmouna, M. *Macromolecules* **1987**, *20*, 1112.
(9) Borsali, R.; Duval. M.; Benmouna, M. *Macromolecules* **1989**, *22*, 816.
(10) Borsali, R.; Duval. M.; Benmouna, M. *Polymer* **1989**, *30*, 610.
(11) Brown, W.; Pu, Z. *Macromolecules* **1990**, *23*, 5097.
(12) Giebel, L.; Borsali, R.; Fischer. E. W.; Benmouna, M. *Macromolecules* **1992**, *25*, 4378.
(13) Kent, M. S.; Tirrell, M.; Lodge, T. P. *Macromolecules* **1992**, *25*, 5383.
(14) Koňák, Č.; Fleischer, G. *Macromolecules* **1997**, *30*, 1457.
(15) Koňák, Č.; Helmstedt, M.; Bansil, R. *Macromolecules* **1997**, *30*, 4342.
(16) Koňák, Č.; Helmstedt, M.; Bansil, R. *Macromolecules* **1998**, *31*, 4639.
(17) Zheng, H.; Teraoka, I. *Macromol. Chem. Phys.*, in press.
(18) Swift, B. W.; de la Cruz, M. O. *Europhys. Lett.* **1996**, *35*, 487.
(19) Xu, Y.; Teraoka, I. *Macromolecules* **1998**, *31*, 4143.
(20) Fujiwara, T.; Kimura, Y.; Teraoka, I. *J. Polym. Sci., Polym. Chem. Ed.* **2000**, *38*, 2405.
(21) Fujiwara, T.; Kimura, Y.; Teraoka, I. *Polymer* **2001**, *42*, 1067.
(22) Provencher, S. W. *Comput. Phys. Commun.* **1982**, *27*, 229.
(23) Doi, M.; Edwards, S. F. *The Theory of Polymer Dynamics*; Oxford University Press: Clarendon, 1986.
(24) Nose, T.; Chu, B. *Macromolecules* **1979**, *12*, 590, 1122.
(25) Rehage, G.; Ernst, O. *Kolloid Z. Z. Polym.* **1964**, *197*, 64.
(26) Rehage, G.; Ernst, O.; Fuhrmann, J. *Discuss. Faraday Soc.* **1970**, *49*, 208.
(27) Cotts, P. M.; Selser, J. C. *Macromolecules* **1990**, *23*, 2050.
(28) Cifra, P.; Bleha, T.; Wang, Y.; Teraoka, I. *J. Chem. Phys.* **2000**, *113*, 8313.
(29) Koch, T.; Strobl, G. R.; Stühn, B. *Macromolecules* **1992**, *25*, 6258.
(30) de Gennes, P. G. *Scaling Concepts in Polymer Physics*; Cornell University Press: Ithaca, NY, 1979.
(31) Brown, W.; Nicolai, T. *Colloid Polym. Sci.* **1990**, *268*, 977.
(32) Fujita, H. *Polymer Solutions*; Elsevier: Amsterdam, 1990.
(33) Hamada, F.; Kinugasa, S.; Hayashi, H.; Nakajima, A. *Macromolecules* **1985**, *18*, 2290.
(34) Kinugasa, S.; Hayashi, H.; Hamada, F.; Nakajima, A. *Macromolecules* **1986**, *19*, 2832.

MA001646E